Reactivity and deactivation mechanisms of pyrolysis chars from bio-waste during catalytic cracking of tar

Maxime Hervy, Elsa Weiss-Hortala, Doan Pham Minh, Hadi Dib, Audrey Villot, Claire Gerente, Sarah Berhanu, Anthony Chesnaud, Alain Thorel, Laurence Le Coq, et al.

Reactivity and deactivation mechanisms of pyrolysis chars from bio-waste during catalytic cracking of tar

Maxime Hervy[a,b,*], Elsa Weiss-Hortala[a], Doan Pham Minh[a], Hadi Dib[a], Audrey Villot[b], Claire Gérente[b], Sarah Berhanu[c], Anthony Chesnaud[c], Alain Thorel[c], Laurence Le Coq[b], Ange Nzihou[a]

[a] *Université de Toulouse, Mines Albi, CNRS, Centre RAPSODEE, Campus Jarlard, Route de Teillet, F.81013 Albi Cedex09, France*
[b] *IMT Atlantique, GEPEA UMR CNRS 6144, 4 rue A. Kastler, CS 20722, 44307 Nantes Cedex 03, France*
[c] *MINES ParisTech, PSL Research University, MAT – Centre des Matériaux, CNRS UMR 7633, BP 87 91003 Evry, France*

HIGHLIGHTS

- Waste-derived char was used as catalyst for tar cracking at different temperatures.
- Chars from food waste and sludge are more efficient than wood-based chars.
- Char deactivation was due to coke deposition and minerals melting/sintering.
- Deactivation mechanism depends on the physicochemical properties of the chars.

GRAPHICAL ABSTRACT

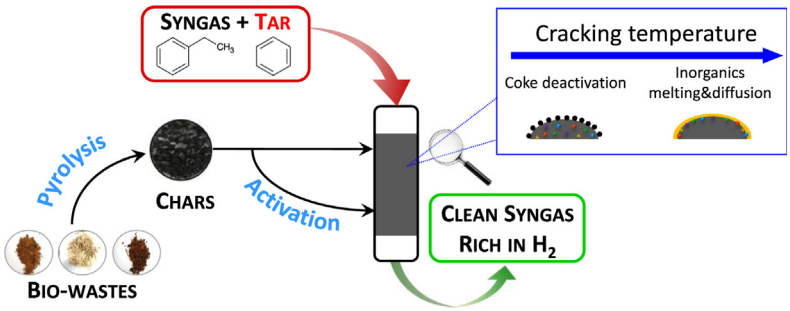

ABSTRACT

The catalytic activity of pyrolysis chars from bio-waste was investigated for the cracking of model tar compounds (ethylbenzene and benzene). Two pyrolysis chars were produced at 700 °C from (1) used wood pallets (UWP), and (2) a 50/50 dry% mixture of food waste (FW) and coagulation-flocculation sludge (CFS). Steam activation at 850 °C was used to study the influence of the porous structure. While coke deposition is known to be responsible for the deactivation of carbonaceous chars and metal catalysts during tar cracking reactions, the deactivation of complex materials such as bio-waste chars has scarcely been studied. For this reason, special attention was paid on the relationships between the physicochemical properties of the chars, the operating conditions, and the deactivation mechanisms. To this aim, the cracking tests were performed over a wide temperature range: 400–650 °C for the ethylbenzene cracking, and 850–950 °C for benzene cracking. After the ethylbenzene cracking tests at 650 °C, the characterisations performed with SEM, BET, FTIR and Raman revealed that coke deposition was responsible for the char's deactivation. The high specific surface area of activated chars explained their higher catalytic activity, and mesoporous catalysts were proved to be more resistant to coke deactivation than microporous catalysts. For these reasons, the higher ethylbenzene conversion (85.8%) was reached with the activated char from food waste and sludge (ac.FW/CFS). For benzene cracking at higher temperature (850 and 950 °C), the chars from food waste and sludge (FW/CFS) were the most active catalysts, despite their

Keywords:
Biochar
Biomass and bio-wastes
Catalysis
Char valorisation
Deactivation
Tar cracking

Abbreviations: UWP, Used Wood Pallets; FW, Food Waste; CFS, Coagulation-Flocculation Sludge; c.UWP, char from UWP; c.FW/CFS, char from a mixture of FW (50 wt.%dry) and CFS (50 wt.%dry); ac., prefix used to name the steam activated chars; EB, ethylbenzene; B, benzene; wt.%, percentage by weight; vol.%, percentage by volume; mol.%, molar percentage

* Corresponding author at: Université de Toulouse, Mines Albi, CNRS, Centre RAPSODEE, Campus Jarlard, Route de Teillet, F.81013 Albi Cedex09, France.
E-mail address: maxime.hervy@mines-albi.fr (M. Hervy).

deactivation by the melting, diffusion and sintering of the inorganic species. This original deactivation mechanism, reported for the first time, led to the formation of an inorganic layer composed of P and Ca species at the char surface, with some areas rich in KCl and NaCl. Non-activated char from food waste and sludge (c.FW/CFS) was surprisingly proved to be more resistant to deactivation by inorganic species than the activated char (ac.FW/CFS) during the benzene cracking tests at 950 °C. This extended catalytic activity was explained by the activation of the non-activated char (c.FW/CFS) with the CO_2 contained in the syngas which simultaneously developed the porosity and created new available active sites. This study marks a step forward in the understanding of the relationships between the deactivation mechanisms, the physicochemical properties of the chars, and the cracking temperature. Finally, a proposal for process integration is presented to consider the possibility to valorise the chars as catalysts to decompose the tar generated in the same pyro-gasification process.

1. Introduction

For the development of a worldwide sustainable energy system reducing the use of fossil fuels and the related greenhouse gas emissions, the contribution of biomass and wastes valorisation technologies is expected to increase in the upcoming years. The pyro-gasification appears as a promising conversion route to produce a gaseous energy carrier named syngas from biomass and waste, by reacting with an oxidizing agent at high temperature (800–1000 °C) [1]. The solid fuel is decomposed in three fractions during the pyro-gasification: syngas, tar, and a solid residue named char. Chars can represent 12–30 wt% of the initial biomass [2]. These solid residues are carbonaceous materials with complex properties [3] and containing several inorganic species [4], depending on the initial waste.

The syngas composition strongly depends on the gasification technology and on the initial fuel composition. The syngas mainly consists of H_2, CO, CO_2, CH_4, and small hydrocarbon species. H_2O and N_2 can also represent significant syngas components, depending on the gasifying agent and on the reactor design. Different types of pollutants can be present in syngas, such as tar, acid gases, and particles [5]. The syngas produced can be valorised in numerous applications with high energy yields (gas turbine, fuel cell, …) or as precursor for the synthesis of high added-value products (chemicals, liquid fuel *via* the Fischer-Tropsch synthesis, …) [6]. However, the syngas must be purified before being valorised in these applications. Tar is the most damaging pollutant which should be removed prior to syngas valorisation [7].

Tar is a complex mixture of condensable aromatic and oxygenated hydrocarbons having a molecular weight higher than benzene (78 g/mol) [8]. Tar can condense at high temperature (below around 350 °C) in the gasification system thus blocking and clogging the downstream equipment [9,10]. The tar concentration can vary between 5 and 200 g Nm^{-3} of syngas [6], and must be reduced to meet the purity standards required for syngas utilisations (tar concentration ranging from 0.01 and 100 mg Nm^{-3}, depending on the end-use [6,11]). Therefore, tar removal from syngas is necessary. Several tar elimination methods have been developed, such as physical treatment (electrostatic precipitation, inertial separation) [12], wet or dry scrubbing [13,14], plasma cracking [15,16], thermal cracking [17–19] and catalytic cracking [20–23]. Cleaning processes can be classified in two types: primary methods aim at limiting the tar formation during the gasification reactions, and secondary methods consist in the collect or decomposition of tar already formed [24]. The catalytic methods consist of the conversion of tar into gases at moderate temperature (400–1000 °C) using catalysts. The catalytic process efficiency was proved to be higher in secondary methods than in primary methods, due to a better control of the syngas cleaning conditions (temperature and residence time) [25]. However, the main drawbacks of the catalytic processes are the cost and the deactivation of the catalysts.

The valorisation of chars as catalysts for tar cracking appears as an attractive approach providing a solution to the main issues of the pyro-gasification process development: (1) find new valorisation routes for the chars [26], and (2) develop an efficient and low-cost syngas cleaning process. Recently, chars from biomass were proved to be promising low-cost catalysts [27–29] or catalyst supports [30–32] for tar cracking. In most of the studies, the operating conditions are specifically selected to obtain chars with suitable characteristics. Activation with steam [33] or carbon dioxide [9] can be performed to enhance the porous structure of the biomass chars. To improve the catalytic activity of these materials, several modifications can be applied, such as metal impregnation and chemical treatment [34]. These modification processes improve the char activity, but also increase the environmental footprint and materials costs. For metal impregnated chars, gaseous species (such as sulfur and chlorine compounds) can be chemically adsorbed on active sites, leading to the catalyst poisoning [35]. Several studies showed that the solid by-product generated by tar cracking reactions (named coke) is responsible for the deactivation of both biomass chars [36] and chars supported catalysts [37]. Indeed, coke is deposited on the catalyst surface thus covering the active sites and clogging the catalyst porous network [38]. Coke is produced during tar cracking by poly-alkylation and condensation of aromatic compounds [39]. Coke could be consumed by gasification reactions catalysed by inorganic species present at the char surface, thus limiting the deactivation process [40,41]. However, inorganic species can also contribute to the catalyst deactivation. For example, silicon can react with alkali metals to form alkali silicates, thus inhibiting their catalytic activity [42]. The sintering of metals, such as ruthenium, can also result in the catalyst deactivation [43]. Due to the chemical complexity of chars from bio-waste, all the above mentioned deactivation mechanisms could simultaneously occur during tar cracking reaction. For this reason, the relationships between the char physicochemical properties, the catalytic temperature, and the deactivation mechanisms must be investigated.

This article studies the catalytic efficiency of various pyrolysis chars from bio-waste for tar cracking. Steam activation was used to improve the porous structure of the pyrolysis chars. Two model tar compounds were selected: ethylbenzene and benzene. In the literature, there is a lack of study devoted to the cracking of light aromatic hydrocarbons other than toluene. Thus, ethylbenzene was chosen as surrogate of light aromatic hydrocarbons (the main class of tar). The catalytic tests were performed at low temperatures (400 and 650 °C) to avoid any additional heat supply downstream of the gasifier for tar cracking. Benzene was also selected as tar surrogate since this molecule is produced in significant amount by tar cracking and gasification reactions [44]. In addition, benzene cracking reaction allows efficiently evaluating the tar cracking activity of the catalysts since benzene is one of the most refractory compounds contained in tar [45]. For these reasons, the benzene cracking tests were performed at higher temperatures (850 and 950 °C). This article aims to study the deactivation mechanisms of various chars during tar cracking reactions, and to better understand their relationships with the initial char properties and cracking temperature. Previous articles studied the removal of tar by pyrolysis chars both produced in the same pyrolysis process [46,47]. In this study, mass balance calculations were also performed to assess the potential *in-situ* valorisation of chars generated in a pyro-gasification system as catalysts for tar cracking. This study is in line with the need to develop a circular economy in waste valorisation and energy production.

2. Materials and methods

2.1. Catalysts production

The bio-waste materials used in this study were from cruise ships and are generated in large amount by modern societies: Used Wood Pallets (UWP), Food Waste (FW) and Coagulation-Flocculation Sludge (CFS). Used Wood Pallets was common softwood (from gymnosperm trees) used in the production of pallets for loading and transportation of food. Food wastes came from feeding activity, and were composed of a mixture of vegetables and animal wastes. Coagulation-Flocculation Sludge was recovered from a wastewater treatment plant present on board the ship.

The pyrolysis was performed at 700 °C during 30 min with a heating rate of 22 °C/min. Two chars were produced: c.UWP, only from UWP, and c.FW/CFS, from a mixture of 50 wt% FW and 50 wt% CFS (on dry basis). The char yields in dry basis were 22 wt% for c.UWP, and 23 wt% for c.FW/CFS. Due to the diameter of the tar cracking reactors, chars were sieved to particle size from 0.5 to 1.6 mm to avoid edge-effects.

A steam activation was applied to the two pyrolysis chars as this process is known to favour the development of micro, meso and macropores [48,49]. Pyrolysis chars were activated at 850 °C during 80 min in a gas atmosphere composed of nitrogen and steam (15 vol%). The solid yield (in dry basis) of the steam activation was 77 wt% for ac.UWP, and 69 wt% for ac.FW/CFS. Solid yield corresponds to the mass of resulting activated char divided by the initial mass of dry char.

2.2. Bio-wastes and chars characterisation

2.2.1. Elemental analysis and ash composition

Prior to elemental analyses, the samples moisture was eliminated at 105 °C while measuring the mass evolution until stabilisation. The elemental composition (C, H, N, S, O) of the samples was determined by using a Thermo Finnigan AE1112 Series Flash. The detection limit of this apparatus was 0.2 wt%. The ash content of the chars was determined by measuring the residual mass after the combustion of 7.0 g of the sample for 15 h in a muffle furnace (Nabertherm P330) at a temperature of 650 °C.

The chemical composition at the overall scale of resulting ash was analysed by X-ray fluorescence spectroscopy (SHIMADZU EDX-800HS). The analyses were performed under vacuum with powdered samples, with a time acquisition of 100 s and a detection limit of 0.001 wt%. The ash was obtained from the combustion of around 20 g of each material. Thus, large samples representative of the materials were analysed which allowed to deal with the chemical heterogeneity of the waste.

Table 1 presents the elemental composition and the ash composition of the different chars. Two types of chars were obtained. Chars from UWP were carbonaceous materials having a carbon content higher than 87 wt%, while chars from FW/CFS were hybrid carbon/mineral materials containing lower carbon content (< 44.1 wt%). The steam activation mainly modified the composition of ac.FW/CFS, with a decrease of the carbon concentration (−11.5%, from 44.1 to 32.6 wt%) and an increase of the ash content (+12.4%, from 47.0 to 59.4 wt%). On the contrary, this activation process did not change the chemical composition of ac.UWP.

The ash composition is presented in Table 1. It can be noted that calcium was the major mineral specie present in the ash of each char (> 34.3 wt%). The ash of UWP-based chars was rich in magnesium and potassium (> 11 wt%), while FW/CFS-based materials contained large amounts of phosphorus (26 wt%) and aluminum (> 13.8 wt%). Among the mineral species, some are known to have a significant catalytic activity in tar cracking reactions: K [50], Ca, P, Fe, Mg [51–53]. On the contrary, the high contents of P and Si could have a detrimental effect on their catalytic activity [42,50,54].

2.2.2. Surface analysis

The chars were characterised by scanning electron microscopy (SEM) using a ZEISS DSM982 microscope equipped with a high-resolution Gemini column, operated at 10–15 kV. Prior to observation, samples were coated with a 2–3 nm Au/Pd layer to ensure electrical conductivity. The local chemical composition at micro-scale was assessed by energy dispersive X-ray spectroscopy (EDX) using a Noran Voyager IV microanalysis system. For each char, several zones were randomly analysed in order to obtain a statistical dataset representative of the materials.

The chemical modification of the char surface due to the tar cracking tests was analysed with FTIR. The samples were crushed and analysed with the Thermo Scientific Nicolet spectroscope using the Attenuated Total Reflectance mode. The resolution was 4.0 cm^{-1} on the wave number range 400–4000 cm^{-1}.

The surface chemistry of fresh and used chars was analysed by Raman spectroscopy. A mapping of the materials surface was performed by analysing 3 regions (of 25 μm^2) of two different particles. A 10 bands deconvolution of the Raman spectra was performed with Matlab® to characterise the carbonaceous structure [55].

2.2.3. Textural properties

The specific surface area and the pore size distribution of the chars were studied by means of nitrogen adsorption-desorption at 77 K using a Micromeritic 3Flex apparatus. Prior each measurement, the samples were outgassed under vacuum (1–30 µm Hg) at 30 °C during at least 16 h. The specific surface area was determined using the BET method, while the HK (Horvath-Kawazoe) and BJH (Barrett, Joyner, Halenda) methods were used to study the microporosity and mesoporosity, respectively. Textural properties of each sample were studied by at least three nitrogen adsorption-desorption isotherms. The average values are listed in Table 2.

The bulk density of the chars was determined using Mercury porosimetry. Measurements were performed using a Micromeritics Autopore IV porometer in a pore size range from 8.5 nm to 600 µm. Prior to analysis, samples were dried in an oven at 105 °C before degassing at 2.75 kPa up to stabilization. For each sample, at least three reproducibility experiments were performed. The mercury volume penetrating the porous structure of the chars was measured at different pressures (from 2.8 kPa to 206.8 10^3 kPa).

Table 1
Elemental analysis and ash composition of the chars.

	c.UWP	ac.UWP	c.FW/CFS	ac.FW/CFS
Elemental analysis (wt%)				
C	87.2 ± 1.0	87.4 ± 1.7	44.1 ± 1.6	32.6 ± 3.1
H	1.8 ± 0.2	0.8 ± 0.1	1.3 ± 0.2	0.9 ± 0.0
N	0.6 ± 0.2	0.4 ± 0.0	3.1 ± 0.1	1.4 ± 0.1
S	*b.d.l.*	*b.d.l.*	*b.d.l.*	*b.d.l.*
O (by difference)	8.3	8.9	4.5	5.7
Ash	2.1 ± 0.1	2.5 ± 0.2	47.0 ± 0.0	59.4 ± 3.4
Ash composition (wt%)				
CaO	42.5	42.2	39.2	34.3
P_2O_5	4.7	4.2	26.2	26.2
K_2O	11.0	13.2	6.4	7.2
Al_2O_3	3.0	2.0	13.8	18.2
Cl	*n.m.*	*n.m.*	7.5	9.2
Fe_2O_3	6.5	3.6	1.6	0.6
SO_3	6.6	6.7	2.7	1.3
SiO_2	8.0	4.4	2.0	2.2
MgO	11.0	13.4	*n.m.*	*n.m.*
Others (TiO_2, MnO, ZnO, CuO, SrO…)	6.7	10.3	0.6	0.8

b.d.l.: below the detection limit (< 0.2 wt%); *n.m.*: non-measured (< 0.001 wt %).

Table 2
Textural analysis of the chars before and after the catalytic tests.

Catalysts	BET specific surface area (m^2/g)	V_{micro} HK (cm^3/g)	V_{meso} BJH (cm^3/g)
c.UWP	51	*n.m.*	*n.m.*
c.FW/CFS	10	0.008	0.016
ac.UWP	625	0.271	0.047
ac.FW/CFS	221	0.100	0.099
ac.UWP_EB	181	0.072	0.366
ac.FW/CFS_EB	13	0.008	0.008
c.FW/CFS_B-950	122	0.059	0.098
ac.FW/CFS_B-950	101	0.049	0.102
ac.UWP_B-950	71	0.036	0.016

n.m.: non-measured.

2.3. Catalytic tests

In this study, two different reactors have been developed to perform the catalytic tests: one for ethylbenzene cracking, and another one for benzene cracking. Indeed, the first system developed to study the ethylbenzene cracking did not allow to accurately measure the evolution of the char bed weight. For benzene cracking tests, the reactor developed allows measuring the evolution of the char weight, and was designed to be high temperature resistant.

2.3.1. Ethylbenzene cracking reactor

The catalytic cracking tests were carried out in a stainless-steel reactor (internal diameter 2.4 cm) placed in an electric furnace in which the heating was monitored by three thermocouples. The model syngas composition and flow rate were controlled by five mass flow meters connected to individual gas cylinders with a purity of 99.995% (H_2, CO, CO_2, CH_4, N_2). Ethylbenzene was introduced in the gas flow by a syringe pump. The cracking tests were performed with an ethylbenzene concentration of 40 g/Nm^3 representative to the tar concentrations in real syngas (5–200 g/Nm^3) [6]. Then, the mixture flowed in a preheater placed in the electric furnace, and entered on the bottom of the reactor (Fig. S.1 in Supplementary Information). The exhaust gas was analysed online with a μ-GC (R-3000, SRA Instruments) and tar cracking products were identified offline using GC–MS (GC–MS Perkin Elmer Auto System XL). Details on the nature of the chromatographic columns and the analysis parameters are given in Table S.1.

The catalytic tests were performed at 400 °C and 650 °C. For both temperatures, the total flow rate was adjusted in order to obtain a gas velocity of 9.6 cm/s in the reactor. At 400 °C, the model syngas was composed of H_2 (30 vol%), CO (40 vol%), CO_2 (15 vol%), N_2 (15 vol%), and the char bed height was 7.0 cm. This syngas composition is representative to real syngas [56–58].

Due to the significant homogeneous cracking reactions occurring at 650 °C with the above-mentioned syngas matrix, a less reactive gas composition was selected: CO (40 vol%) and N_2 (60 vol%). This gas matrix permitted to quantify the amount of permanent gases (H_2, CO_2, CO, CH_4, N_2, C_xH_y) produced by ethylbenzene cracking reactions. In order to reduce the experiment duration time, the bed height was reduced from 7.0 cm to 4.5 cm for the tests at 650 °C. Since the gas velocity was kept constant (9.6 cm/s), the residence time of the gas in empty column was 0.67 s at 400 °C, and 0.47 s at 650 °C. The closure system of this column did not allow to precisely measure the bed mass evolution.

Two repetitions were performed with ac.UWP and ac.FW/CFS at 650 °C. The relative deviation of the average ethylbenzene conversion was lower than 8% for ac.UWP, and lower than 2% for ac.FW/CFS.

2.3.2. Benzene cracking reactor

The benzene catalytic cracking tests were carried out in a quartz reactor (internal diameter 2.4 cm) placed in an electric furnace (Fig. S.2 in Supplementary Information), and were performed at 850 °C and 950 °C in order to compare the results with a recent study [9].

While ethylbenzene was significantly decomposed by homogenous reactions due to the presence of H_2, the thermal conversion of benzene was zero at 850 and 950 °C with the presence of a model syngas (H_2 (30 vol%), CO (40 vol%), CO_2 (15 vol%), CH_4 (10 vol%), and N_2 (5 vol %)). The thermal conversion was measured under the catalytic conditions but with empty reactor (without catalyst). This result confirmed that no benzene conversion due to homogeneous reactions occurred, even in the presence of a reactive model syngas. Benzene was introduced in the syngas flow by a syringe pump at a concentration of 35 g/Nm^3. The mixture was preheated in an external preheater, and entered on the bottom of the quartz reactor. The exhaust gas was analysed online with a μ-GC (My-GC, SRA Instruments) (Table S.1). Compared to the syngas used for ethylbenzene cracking tests at 400 °C, methane was added in the mixture to investigate the possible dry reforming reaction that can occur at high temperature.

The bed height of chars was set at 4.5 cm. For both temperatures, the total flow rate was adjusted in order to obtain a gas velocity of 9.6 cm/s in the reactor and a residence time of the gas in empty column of 0.47 s. This configuration allowed to precisely measure the mass evolution of the char bed. The three catalysts having the higher catalytic activity for ethylbenzene conversion were used for benzene cracking.

Two repetitions were performed with the three chars at 950 °C. The relative deviation of the average benzene conversion was lower than 3% for the three chars.

2.3.3. Experimental data evaluation

During the tar cracking reactions, the volumetric flow rate at the reactor outlet could vary. To address this, the nitrogen placed in the model syngas was used as a passive tracer allowing the calculation of the real output volumetric flow rate of syngas ($Q_{v_{tot}}^{out}$).

The average tar conversion (X_j) was defined as the molar difference of tar (ethylbenzene or benzene, named *j*) leaving the reactor (n_j^{out}) to the amount of tar fed into the reactor (n_j^{in}) over a given time.

$$X_j = \frac{n_j^{in} - n_j^{out}}{n_j^{in}} \cdot 100 \quad (1)$$

The composition of the tar cracking products (named *i*) was discussed based on the molar selectivity (Sel_i), calculated with Eq. (2):

$$Sel_i = \frac{n_{prod,i}^{out}}{\sum n_{prod}^{out}} \cdot 100 \quad (2)$$

where $n_{prod,i}^{out}$ is the molar amount of the tar cracking product *i* at the reactor outlet.

For the benzene cracking experiments, the evolution of the bed mass after the catalytic tests (Δm_{bed}) was calculated:

$$\Delta m_{bed} = \frac{m_{bed}^{in} - m_{bed}^{fin}}{m_{bed}^{in}} \cdot 100 \quad (3)$$

with m_{bed}^{in} and m_{bed}^{fin} the initial bed weight and the final bed weight (in g).

In addition, the evolution of the carbon weight contained in the char before and after the benzene cracking tests (Δ_{carbon}) was calculated:

$$\Delta_{carbon} = \frac{(m_{bed}^{fin} * [C]_{char}^{fin}) - (m_{bed}^{in} * [C]_{char}^{in})}{m_{bed}^{in} * [C]_{char}^{in}} \cdot 100 \quad (4)$$

With $[C]_{char}^{in}$ and $[C]_{char}^{fin}$ the initial and final carbon content of the char (in wt.%).

3. Results and discussion

3.1. Catalytic performances of the chars

3.1.1. Ethylbenzene conversion

Light aromatic hydrocarbons are the main class of tar contained in syngas. To cope with the lack of study in the literature devoted to the cracking of light aromatic hydrocarbon molecules other than toluene, ethylbenzene was chosen as model molecule. The tests were performed at two temperatures (400 °C and 650 °C), corresponding to the entrance temperature of the Fischer-Tropsch synthesis and the usual outlet temperature of the gasification reactor, respectively. In these conditions, no supplementary heat source would be required for the syngas cleaning process. It should be kept in mind that the model syngas was composed of H_2 (30 vol%), CO (40 vol%), CO_2 (15 vol%), and N_2 (15 vol%) for the tests performed at 400 °C. At 650 °C, a less reactive gas mixture was used to limit the homogeneous cracking reactions: CO (40 vol%) and N_2 (60 vol%).

Fig. 1 presents the evolution of ethylbenzene conversion during the catalytic tests performed at 400 °C. Fig. S.3A (in Supplementary Information) displays the average conversion of ethylbenzene (EB) achieved with the different chars at 400 °C and during the thermal cracking test (horizontal line). The average conversions were calculated within the 80 first minutes of experiments as all the catalysts were totally deactivated after 80 min (Fig. 1). At this reduced temperature, the ethylbenzene conversion during thermal cracking test (in empty reactor) was 11.0%, and the catalytic activity of the chars was low. Indeed, the ethylbenzene conversions obtained were: 21.6% for ac.FW/CFS > 16.6% for ac.UWP > 13.3% for c.FW/CFS > 10.9% for c.UWP. It can be noted that the activated chars presented higher ethylbenzene conversion than the pyrolysis chars.

To achieve higher conversion, the tests were performed at 650 °C. The evolutions of the ethylbenzene conversion (X_{EB}) and of the reaction products selectivity during the cracking tests are presented in Fig. 2. The less reactive char (c.UWP) was deactivated after 85 min. To compare the catalytic activity of each catalyst, the average conversions (X_{EB}) were calculated within the 85 first minutes of experiment. In these conditions, the thermal conversion reached 37.2 wt%. At this temperature, the catalytic activity of the chars was 4 to 5.8 times higher than that obtained at 400 °C (Fig. S.3B in Supplementary Information). Within 85 min, the catalysts can be ranked in ascending order of their effectiveness according to ac.FW/CFS (85.8%) > ac.UWP (77.3%) > c.FW/CFS (77.2%) > c.UWP (53.2%). Almost similar conversion was obtained with ac.UWP and c.FW/CFS. This latter appears as an attractive material due to its significant catalytic activity without the need for additional steam activation.

To investigate the deactivation kinetic, the evolutions of the ethylbenzene conversion (X_{EB}) and of the reaction products selectivity were studied (Fig. 2). The four chars presented different catalytic behaviour. The char c.UWP was the less reactive char, with an ethylbenzene conversion lower than 20% after 40 min of test. During the first 30 min, the chars c.FW/CFS and ac.UWP were more active than ac.FW/CFS. Over the same period, H_2 and CO_2 were the main reaction products generated by ethylbenzene decomposition over these two chars, while styrene was produced in significant amount by ac.FW/CFS. The products selectivity demonstrates that the catalytic activity of chars promotes the conversion of tar into hydrogen, which increases the syngas quality, as shown in a previous study [59]. Only 2 mol.% of the ethylbenzene was converted into benzene, which is stable at this temperature. For a prolonged test duration, the deactivation rate was faster for c.FW/CFS > ac.UWP > ac.FW/CFS (Fig. 2). Thus, after 170 min of test, the average ethylbenzene conversion was 57.0% for c.FW/CFS, 65.4% for ac.UWP, and 78.5% for ac.FW/CFS.

The catalytic activity of the three most efficient catalysts (ac.FW/CFS, ac.UWP and c.FW/CFS) for the cracking of a thermally stable molecule (benzene) as well as the influence of high temperatures (850–950 °C) on the deactivation mechanisms were studied in the next section.

3.1.2. Benzene conversion

Benzene is the most important hydrocarbon molecule produced by gasification and tar cracking reactions. As benzene is known for its thermal stability, studying its cracking is interesting to evaluate the catalyst efficiency. Temperatures significantly higher than 650 °C must be used to observe benzene cracking. To compare our results with previous studies, the benzene cracking tests were performed at 850 and 950 °C. The model syngas was composed of H_2 (30 vol%), CO (40 vol%), CO_2 (15 vol%), CH_4 (10 vol%), and N_2 (5 vol%). Even with this reactive gas matrix, the thermal decomposition of benzene (without catalyst) at both temperatures was 0%.

As the less reactive char was deactivated after 60 min of test at 850 °C, the average conversions of benzene were calculated within this period of time. The values of these average conversions are presented in Fig. S.4 (in Supplementary Information). The evolutions of the benzene conversion versus time are presented in Fig. 3.

It can be noted that rising temperature from 850 to 950 °C increased the catalytic activity of the three catalysts, especially for FW-CFS-based chars (Fig. 3). At 850 °C, the two activated chars were the most efficient catalysts for benzene cracking, with a maximum conversion for ac.FW/CFS (48.4%) (Fig. S.4A). The conversion obtained with ac.UWP and c.FW/CFS were 34.3%, and 16.6%, respectively. At 950 °C, the reactivity of ac.UWP was barely increased (from 34.3 to 36%). However, the catalytic activity of c.FW/CFS increased from 16.6 to 46.2%, and that of ac.FW/CFS rose from 48.4 to 82.4%. This result is in disagreement with *Morgalla et al.* [60] who observed a detrimental effect of rising temperatures (from 900 to 1100 °C) on the benzene conversion over chars, mainly attributed to the char gasification reaction with steam.

Our results are compared to previous articles obtained under comparable conditions. The benzene conversion at 900 °C over a packed bed of alumina loaded with 35 g Nm^{-3} of biomass char particles in a mixture nitrogen-steam (13.5 vol%) was around 55% for *Morgalla et al.* [60]. *Burhenne et al.* [9] studied the catalytic activity of spruce wood chars pyrolysed and activated with CO_2 for benzene cracking. The tests were performed in N_2 atmosphere between 850 and 1050 °C, with residence time higher than that used in our study (0.80 s against 0.45 s, respectively). The higher benzene conversion at 950 °C within the 60 first minutes of test was 52%, achieved with a char pyrolysed at 500 °C and then activated at 900 °C. In the present study, the average benzene conversion within the 60 first minutes of test was 82% with ac.FW/CFS, 46.2% with c.FW/CFS, and 36.0% with ac.UWP. This result shows that FW/CFS-based chars are promising catalysts for tar cracking.

The deactivation kinetics were proved to strongly depend on the cracking temperature and on the char properties. At 850 °C, the three catalysts presented different deactivation behaviours (Fig. 3A). c.FW/CFS was rapidly deactivated during the first 10 min, and maintained a

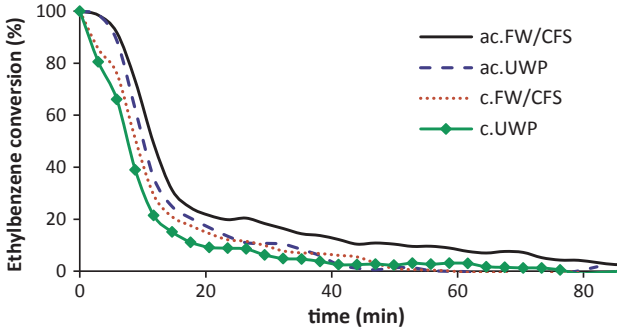

Fig. 1. Evolution of the ethylbenzene conversion over time during the catalytic tests performed at 400 °C.

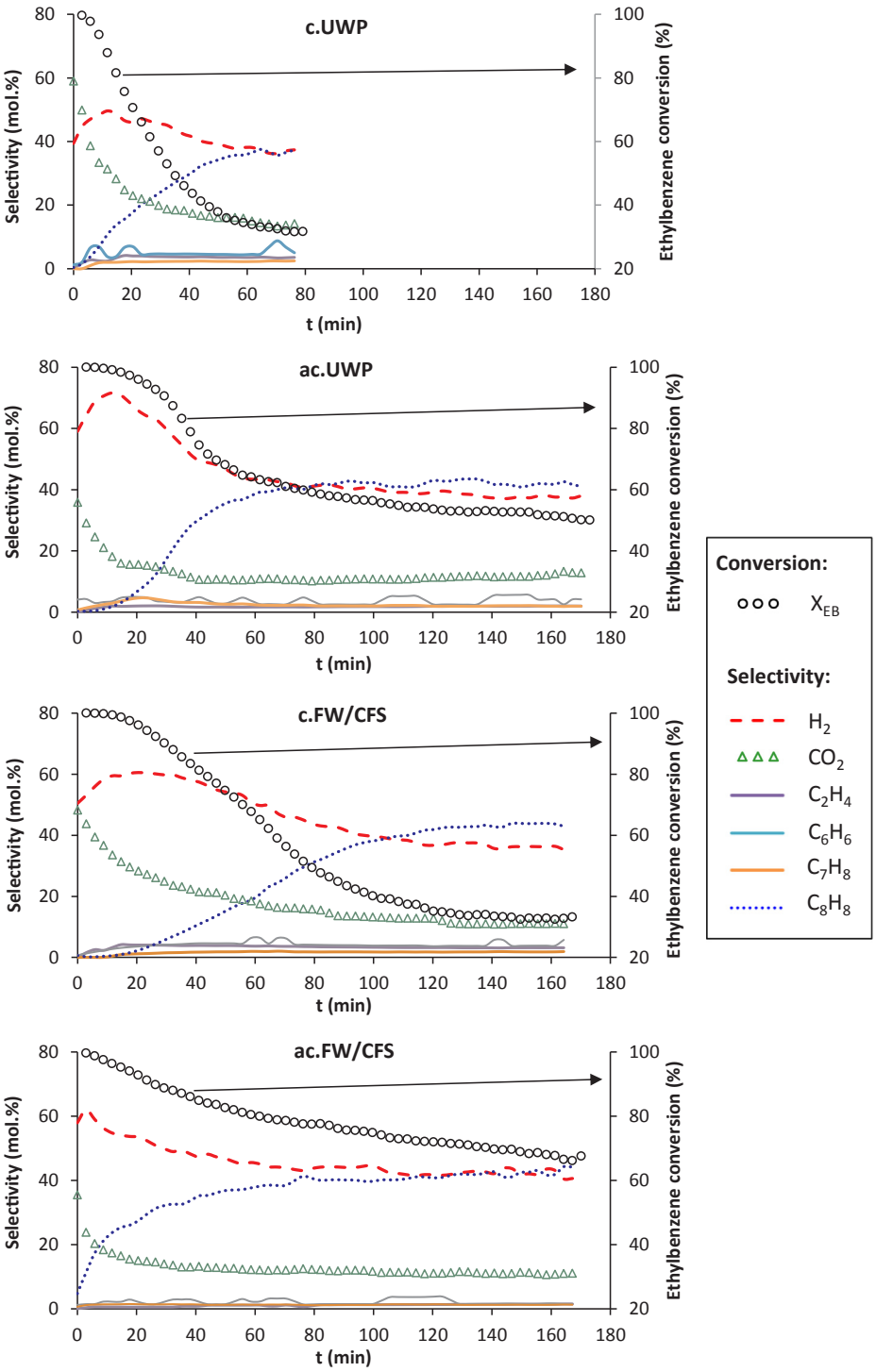

Fig. 2. Evolution of the ethylbenzene conversion and the selectivity of the reaction products over time during the catalytic tests performed at 650 °C.

low catalytic activity up to 40 min. The deactivation of ac.UWP was linear, while the deactivation rate of ac.FW/CFS progressively decreased during the catalytic test (Fig. 3A).

At 950 °C, the deactivation behaviour was different from that obtained at 850 °C (Fig. 3B). The deactivation of ac.FW/CFS was linear over the catalytic test duration (500 min). On the contrary, the deactivation kinetics of both ac.UWP and c.FW/CFS had two distinct phases. The first phase consisted in a drastic drop of the catalytic activity within the first 60 min. After this drop, c.FW/CFS maintained a benzene conversion higher than 20% up to 300 min. On the contrary, ac.UWP was completely deactivated after 220 min.

When the average conversion at 950 °C is calculated over 500 min of test, the order of char efficiency is modified: c.FW/CFS (23.0%) > ac.FW/CFS (18.5%) > ac.UWP (6.9%). The higher conversion obtained with c.FW/CFS is explained by its slow deactivation between 60 and 500 min. To better understand these evolutions, the relationships between the physicochemical properties of the char and the deactivation mechanisms were investigated by several characterisations.

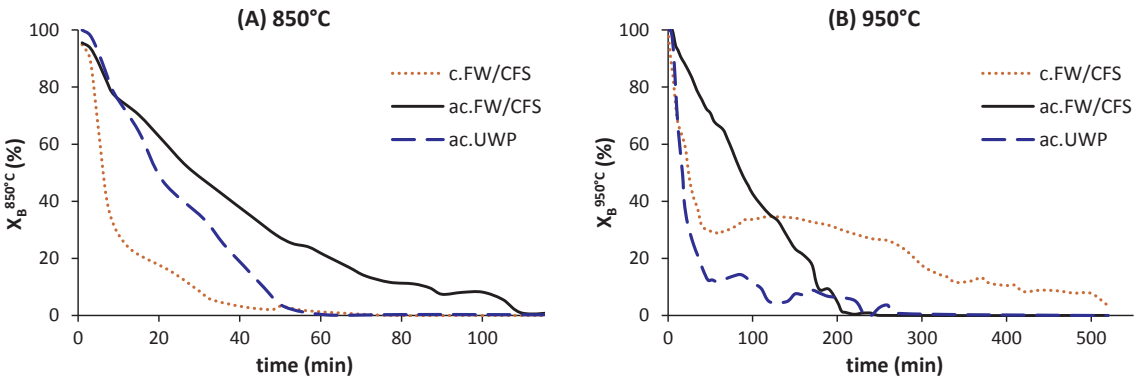

Fig. 3. Evolution of the benzene conversion over time for the three most efficient catalysts at: (A) 850 °C, and (B) 950 °C.

3.2. Deactivation mechanisms

3.2.1. Deactivation during ethylbenzene cracking at 650 °C

In order to identify the phenomena responsible for the catalysts deactivation during ethylbenzene cracking tests at 650 °C, the two most efficient chars (ac.UWP and ac.FW/CFS) were characterised after the catalytic tests, and were named with the suffix "_EB".

The surface of the activated chars was observed using SEM. The results show that the initial surface of both chars is mainly carbonaceous with some inorganic particles deposited (Fig. 4A, B, E, F). After the catalytic tests, the surface is covered by a disorganised carbonaceous matter (Fig. 4C, D, G, H). The two chars were produced at higher temperature than that used for the ethylbenzene cracking tests (850 °C against 650 °C, respectively). Thus, the modification of the surface cannot be induced by thermal effects. The apparition of this carbonaceous matter suggests the deposition of coke generated during the ethylbenzene cracking reactions. Indeed, coke deposition is well known for catalyst deactivation during tar cracking [36].

The evolution of the textural properties during the ethylbenzene decomposition was analysed by nitrogen adsorption-desorption at 77 K. Initially, the pyrolysis chars c.FW/CFS and c.UWP had low specific surface area (10 and 51 m^2/g, respectively) and the analysis of their textural properties with nitrogen adsorption-desorption was not accurate. The steam activation substantially increased the porosity of the chars. The specific surface area of ac.UWP and ac.FW/CFS reaches 625 and 221 m^2/g, respectively. The results summarised in Table 2 reveal a drastic reduction of the specific surface area after the EB cracking tests: −71% for ac.UWP_EB, and −94% for ac.FW/CFS_EB. The decrease of the specific surface area is explained by the carbon deposition observed with SEM, and confirms that coking was responsible for the char deactivation. For FW/CFS-based chars, the increase in carbon content after the ethylbenzene cracking tests was confirmed by elemental analysis (Table S.2 in Supplementary Information).

The textural properties are a key parameter in the kinetics of deactivation by coking. Although c.FW/CFS had low surface area, this char presented high catalytic activity for ethylbenzene cracking during the first minutes of test at 650 °C (Fig. 2). However, due to its low surface area (10 m^2/g), c.FW/CFS was quickly deactivated by the coke deposition covering its surface and preventing the access of tar to the active sites. The higher specific surface area of the activated chars explains their extended catalytic activity for ethylbenzene conversion at 650 °C. Indeed, the coke is "stored" in the porous volume which increases the time needed to totally cover the char surface. This conclusion is in agreement with the results published by *Drago et al.* [61]. The pore size is also involved in the deactivation kinetics by coke deposition. The char ac.UWP has the highest specific surface area (625 m^2/g) and its porous volume contains 85% of micropores (Table 2). On the contrary, ac.FW/CFS has lower specific surface area (220 m^2/g) and is mainly mesoporous (50% of the porous volume). Thus, the micropores of ac.UWP were clogged faster by coke deposition than the mesopores of ac.FW/CFS. For this reason, ac.FW/CFS had an extended catalytic activity [62]. In addition, the large amount of mineral species contained in ac.FW/CFS can catalyse the gasification reactions of coke, contributing to the slower deactivation of this char [36,63,64].

The modifications of the surface chemistry were analysed by FTIR and Raman spectroscopies. Fig. 5 highlights the chemical modifications underwent by activated chars during the ethylbenzene cracking experiment at 650 °C. The surface of ac.FW/CFS was initially rich in a mineral phase having transmission peaks at 1030, 600 and 550 cm^{-1} (peaks α in Fig. 5A). This mineral phase was identified as

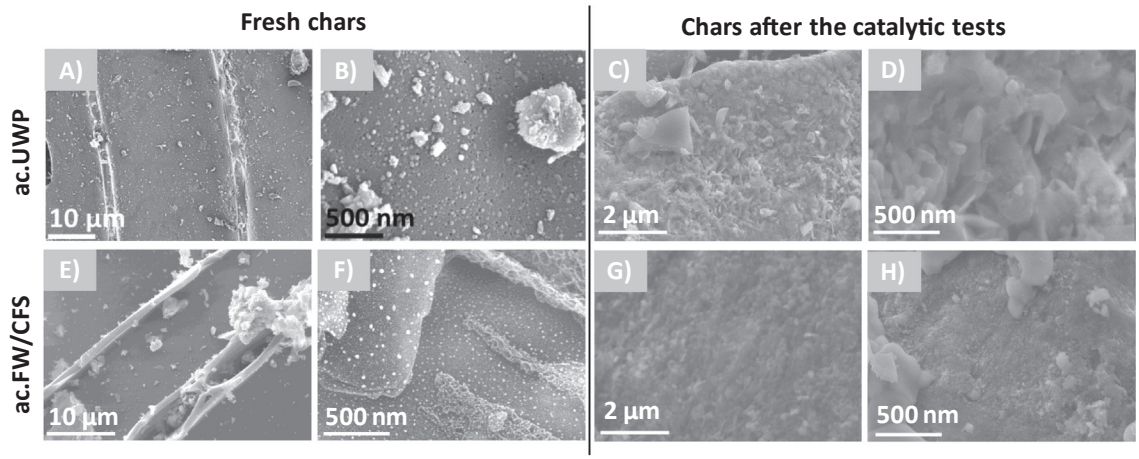

Fig. 4. SEM images of the activated chars ac.UWP and ac.FW/CFS before and after the ethylbenzene cracking tests at 650 °C.

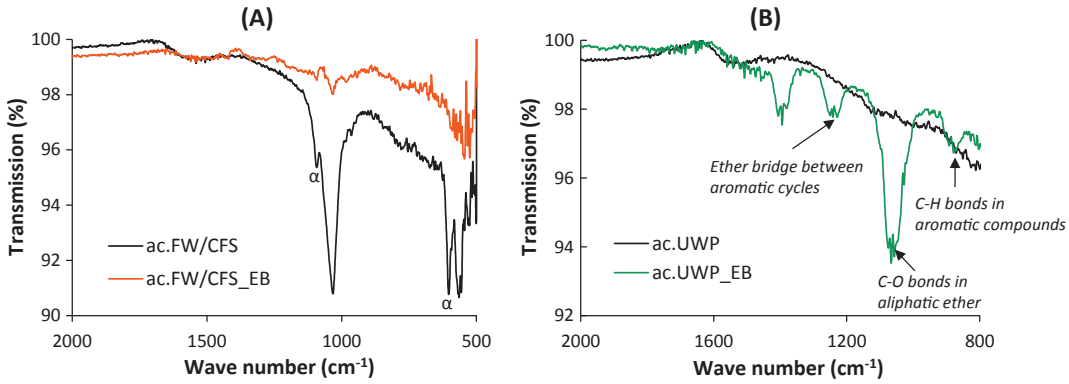

Fig. 5. Transmission FTIR spectra of the activated chars before and after the ethylbenzene cracking tests at 650 °C: (A) ac.FW/CFS, and (B) ac.UWP.

hydroxyapatite ($Ca_{10}(PO_4)_6(OH)_2$). After the tests, the mineral signal decreases, which can be ascribed to the coke deposition on the surface. For ac.UWP (Fig. 5B), new transmission peaks appear after the catalytic tests at wave numbers of 1380, 1240, 1050 and 870 cm^{-1}. These peaks correspond to the bending of C—H bonds in aromatic compounds (870 cm^{-1}), and ether bridge between aromatic cycles (1240 cm^{-1}). The most intense peak at 1050 cm^{-1} corresponds to C—O bonds in aliphatic ether. Thus, FTIR spectra indicate that the coke deposited on the ac.UWP_EB surface is mainly aliphatic. The aliphatic nature of this coke was also studied by Raman spectroscopy.

The deconvolution of the experimental Raman spectra allows a precise description of the carbonaceous matrix. The complete analysis of the carbon matrix of these chars was already reported in a previous article [57]. The results listed in Table 3 confirm the chemical modification of the carbonaceous surface of ac.UWP during the catalytic tests. Indeed, ac.UWP_EB presents a less organised structure than ac.UWP with a decrease of the graphene-like structures (drop of 20% of the $(I_G + I_D)/I_{tot}$ ratio). On the contrary, the proportion of small aromatic systems ($(I_{Gr} + I_{Vl} + I_{Vr})/I_{tot}$) and aliphatic structures (I_S/I_{tot}) increases drastically. These results corroborate the FTIR analysis and confirm the aliphatic nature of the coke deposited on the surface of ac.UWP during the ethylbenzene cracking tests.

Coking is clearly identified as the phenomenon responsible for catalysts deactivation during ethylbenzene cracking at 650 °C. The deactivation mechanism occurring during benzene decomposition at higher temperatures (850 and 950 °C) was also investigated.

3.2.2. *Deactivation during benzene cracking at 850 and 950 °C*

The chars were characterised after the benzene cracking tests, and were named with the suffix "_B". First, the textural properties were analysed by nitrogen adsorption-desorption at 77 K. The results presented in Table 2 show that the specific surface area of activated chars decreased drastically during the benzene cracking tests at 950 °C (from 625 to 122 m^2/g for ac.UWP, and from 221 to 101 m^2/g for ac.FW/CFS), while it increased substantially for c.FW/CFS (from 10 to 122 m^2/g).

Table 4 presents the evolution of the catalytic bed weight after the benzene cracking tests (Δm_{bed}). For ac.UWP, the weight of the catalytic bed slightly increased at 850 °C and was constant at 950 °C. On the contrary, the weight of ac.FW/CFS decreased by 8% at both temperatures, and was significantly higher with c.FW/CFS (−19.8% and −22.8% at 850 and 950 °C, respectively). Since the cracking temperature (850 and 950 °C) was higher than the temperature of the char production, the volatilisation of heteroatoms (N, H and O) and of some mineral species can be responsible for the mass loss of the catalytic bed observed for FW/CFS-based chars. As the non-activated char c.FW/CFS was produced at lower temperature (700 °C), this thermal effect is even more significant and explains the higher mass loss (−19.8 and −22.8%). The volatilisation of heteroatoms from FW/CFS chars during benzene cracking tests is confirmed by the elemental analysis (Table 4), revealing a significant decrease in H and N contents with rising temperature. In addition, activation of the carbonaceous matrix with CO_2 contained in the syngas is expected to occur, especially for the non-activated char (c.FW/CFS). CO_2 activation likely contributes to the mass loss of the catalysts, and to the increase of the specific surface area of c.FW/CFS during the benzene cracking test (from 10 to 122 m^2/g).

Mass balance was performed to calculate the evolution of the weight of carbon contained in the chars before and after the benzene cracking tests (Δ_{carbon}). The results, presented in Table 4, confirm that CO_2 activation of the c.FW/CFS carbonaceous matrix occurred during the benzene conversion tests, since the weight of carbon decreased by 16.6 and 29.5% at 850 and 950 °C, respectively. Thus, coke deposition is not likely to be responsible for the c.FW/CFS deactivation. For ac.FW/CFS, Δ_{carbon} slightly decreased during the benzene cracking test at 850 °C, while it significantly increased at 950 °C. This result suggests that ac.FW/CFS deactivation did not result from coke deposition at 850 °C. Additional characterisations were performed to elucidate the deactivation mechanism of FW/CFS-based chars.

The surface of FW/CFS-based chars was studied by SEM. SEM images of ac.FW/CFS before (Fig. 6A–D) and after the benzene cracking tests at 950 °C (Fig. 6E–H) reveal a strong modification of the surface. After the catalytic tests, a layer of mineral matter covering the char surface is observed. A wide range of mineral structures appeared, such as homogeneous layer (Fig. 6G and H), needles (Fig. 6F), beads (Fig. 6F) or cubic crystals (insert on Fig. 6G). Similar observations were made on the surface of c.FW/CFS_EB-950 (Fig. S.5 in Supplementary

Table 3
Ratio definition of the Raman spectra and deconvolution results obtained with ac.UWP and ac.UWP_EB.

Ratio (%)	Description	ac.UWP	ac.UWP_EB
I_G/I_{tot}	Graphene sheets and graphene-like sheets	24.4	14.1
I_D/I_{tot}	Imperfections in graphene-like sheets and large aromatic rings systems (≥6 rings)	36.3	26.2
$(I_{Gr} + I_{Vl} + I_{Vr})/I_{tot}$	Small aromatic rings systems (3–5 rings)	23.3	34.6
I_S/I_{tot}	sp^2-sp^3 carbonaceous structures, aliphatic structures	10.0	12.9
$(I_{Gl} + I_{Sl} + I_{Sr} + I_r)/I_{tot}$	Minor structures	6.0	12.2
$(I_G + I_D)/I_{tot}$	Total graphene-like structures	60.7	40.3

Table 4
Elemental analyses of the chars before and after the benzene cracking tests, and evolution of the catalytic bed weight (Δm_{bed}) and of the weight of carbon contained in the char (Δ_{carbon}).

Materials	C (wt.%)	H (wt.%)	N (wt.%)	S (wt.%)	O (wt.%)	Ash (wt.%)	Δm_{bed} (wt.%)	Δ_{carbon} (wt.%)
c.FW/CFS	44.1 ± 1.6	1.3 ± 0.2	3.1 ± 0.1	*b.d.l.*	4.5	47.0 ± 0.0	*n.m.*	*n.m.*
c.FW/CFS_B-850	45.9 ± 1.0	0.5 ± 0.0	1.7 ± 0.1	*b.d.l.*	*n.m.*	*n.m.*	−19.8	−16.6
c.FW/CFS_B-950	40.3 ± 2.3	0.3 ± 0.0	0.5 ± 0.1	*b.d.l.*	6.8	52.1 ± 2.3	−22.8	−29.5
ac.FW/CFS	32.6 ± 3.1	0.9 ± 0.0	1.4 ± 0.1	*b.d.l.*	5.7	59.4 ± 3.4	*n.m.*	*n.m.*
ac.FW/CFS_B-850	34.4 ± 0.7	0.4 ± 0.0	0.8 ± 0.0	*b.d.l.*	*n.m.*	*n.m.*	−8.0	−2.9
ac.FW/CFS_B-950	42.1 ± 1.7	0.4 ± 0.1	0.7 ± 0.1	*b.d.l.*	/	59.7 ± 0.3	−8.1	+18.7
ac.UWP	87.4 ± 1.7	0.8 ± 0.1	0.4 ± 0.0	*b.d.l.*	8.9	2.5 ± 0.2	*n.m.*	*n.m.*
ac.UWP_B-850	93.4 ± 0.6	0.7 ± 0.1	0.72 ± 0.2	*b.d.l.*	*n.m.*	*n.m.*	+2.2	+9.4
ac.UWP_B-950	92.9 ± 0.2	0.5 ± 0.0	0.5 ± 0.0	*b.d.l.*	5.7	2.5 ± 0.2	0.0	+6.3

b.d.l.: below the detection limit (< 0.02 wt%), *n.m.:* non-measured.

Information). SEM-EDX analyses specify that the inorganic layer is mainly composed of phosphorus and calcium, with some areas rich in KCl and NaCl. These observations demonstrate that the deactivation of FW/CFS-based chars originates from the melting, diffusion and sintering of inorganic species containing phosphorus towards the surface, thus covering the active mineral species (Ca, K, Al, …) and inhibiting their catalytic effect. The encapsulation of active mineral species by phosphorus-containing compounds during thermal treatment was already reported by *Hognon et al.* [65]. P-compounds, such as KPO_3 or KH_2PO_4, can melt a relatively low temperature and form a liquid phase [66,67]. The presence of Na and K is also expected to promote the melting phenomenon, since these compounds are known to decrease the ashes melting point [68,69]. The significant amount of Cl in FW/CFS-based chars can promote the volatilisation of alkali metals that can further react with compounds rich in phosphorous to form low eutectic species [70]. The latter can then be deposited on the char surface and form a sticky layer.

The extended catalytic activity of c.FW/CFS for benzene cracking at 950 °C compared to ac.FW/CFS is explained by two competitive effects. On the one hand, the melting, diffusion and sintering of inorganic compounds towards the surface inhibit the catalytic efficiency of active mineral species. On the other hand, the activation of c.FW/CFS by the carbon dioxide of the model syngas simultaneously develops the porosity and created new available active sites. A simplified deactivation scheme of c.FW/CFS is proposed in Fig. 7. For ac.FW/CFS, the deactivation by inorganic species melting and diffusion is faster than for c.FW/CFS, since the carbonaceous matrix had already been activated with steam. Thus, coke deposition occurs and explains the increase in Δ_{carbon} at 950 °C (+18.7 wt%).

In order to understand the slight increase of ac.UWP bed weight at 850 °C and its constant value at 950 °C, together with the drastic drop of its specific surface area, its elemental composition was analysed after the benzene cracking tests. The results listed in Table 4 reveal a significant increase of the carbon content (+5.5%), while heteroatoms concentration (hydrogen and oxygen) decreased by 3.4%. The weight of carbon contained in ac.UWP significantly increased during the benzene conversion. Δ_{carbon} rose by 9.4 and 6.3% at 850 and 950 °C, respectively. These properties evolutions indicate that ac.UWP was deactivated by the deposition of coke generated by benzene cracking reactions. The mass loss resulting from the volatilisation of heteroatoms due to the thermal effect was offset by the coke deposition, thus explaining the constant or increasing weight of ac.UWP bed. It can be noted that the coke production is expected to increase with rising temperature, since polymerisation and condensation reactions are promoted by high temperatures [71]. However, the catalytic activity of ac.UWP was higher at 950 °C. This result is explained by the fact that the reaction of coke gasification with CO_2 is more intensively promoted than coke producing reactions at 950 °C [72].

3.3. Process integration

To consider the possibility to valorise chars as catalysts to decompose the tar generated in the same pyro-gasification process, mass balance calculations including the catalytic activity of each char are completed. Fig. 8 illustrates the process configuration considered. As benzene is not a problematic molecule for the syngas valorisation in gas engine [73], the calculations are based on the catalytic results of ethylbenzene decomposition at 650 °C (the surrogate of light aromatic hydrocarbons) and suppose a continuous reactor. Tar removal capacity of char $\left(\frac{x}{m}\right)_{char}$ corresponds to the amount of ethylbenzene removed from the syngas with 1 kg of chars at 650 °C (Eq. (5)).

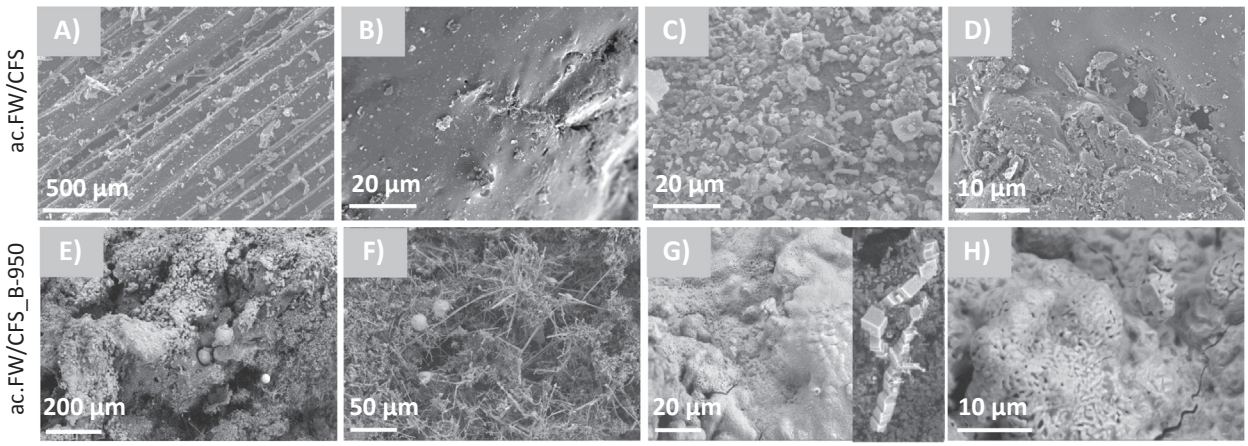

Fig. 6. SEM images of ac.FW/CFS before and after the benzene cracking tests at 950 °C.

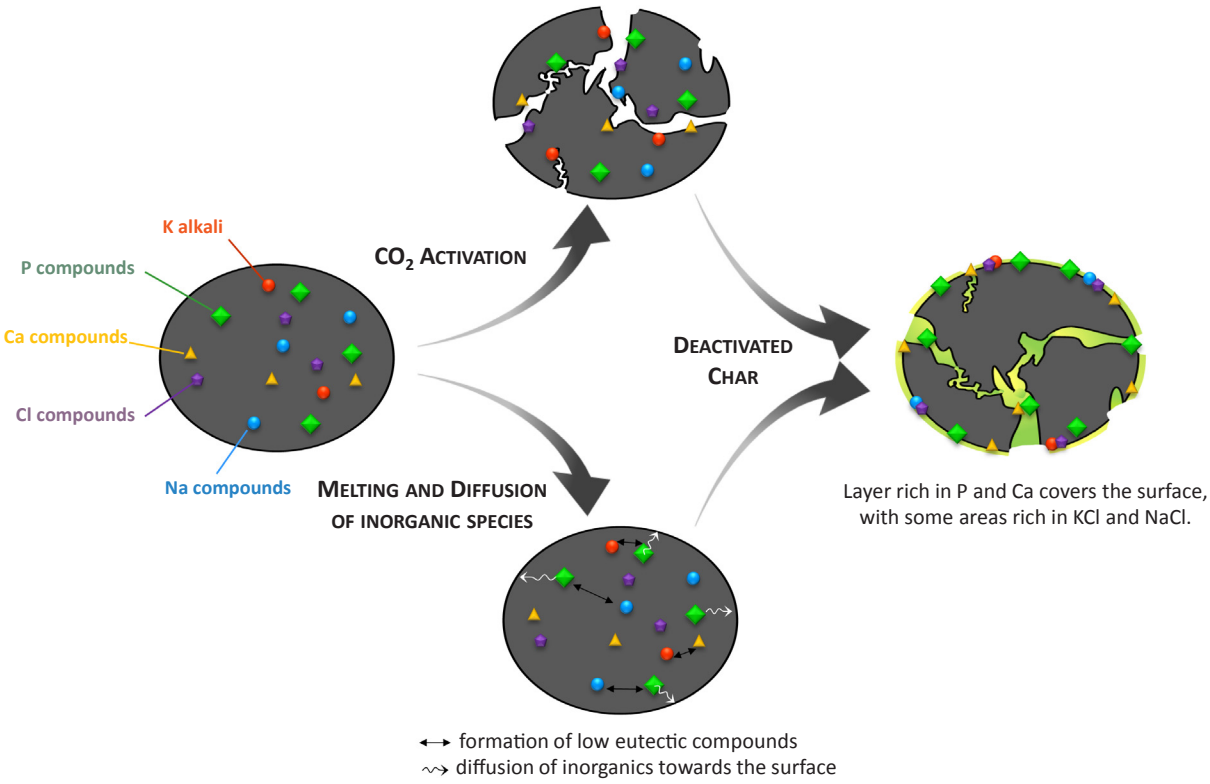

Fig. 7. Competitive phenomena occurring during the benzene cracking test with c.FW/CFS.

$$\left(\frac{x}{m}\right)_{char} = \sum_{0}^{C} \frac{(Q_m EBin - Q_m EBout)}{m_{catalytic\ \ bed}} \tag{5}$$

where $Q_m EBin$ and $Q_m EBout$ are the mass flow rate of ethylbenzene at the inlet and outlet of the catalytic bed, respectively.

As the ethylbenzene cracking tests were stopped before the total deactivation of the chars for reasons of time, the removal capacities of the catalysts were determined within the period for which the ethylbenzene concentration in the exhaust gas was between 0 and 20 g Nm^{-3}. The global tar removal capacity ($\left(\frac{x}{m}\right)_{waste}$, Eq. (6)) expresses the amount of ethylbenzene removed with chars produced from 1 kg of initial waste.

$$\left(\frac{x}{m}\right)_{waste} = \left(\frac{x}{m}\right)_{char} * \eta_{char} \tag{6}$$

The char yield (η_{char}) corresponds to the dry mass of resultant char obtained from 100 g of dry initial bio-waste (Eq. (7)).

$$\eta_{char} = \frac{m_{char}}{m_{initialwaste}} * 100 \tag{7}$$

For the mass balance calculations, values representative of conventional bio-waste gasification are selected: a syngas yield of 3.5 Nm^3 of syngas/kg of bio-waste, and a tar concentration of 60 g Nm^{-3}. In these conditions, 1 kg of bio-waste would generate 210 g of tar after gasification. This value represents the tar input in the tar cracking reactor (see Fig. 8).

Table 5 presents the char yield, the bulk density of the chars measured with mercury porosimetry, and the different tar removal capacities determined for ethylbenzene cracking at 650 °C. The global tar removal capacity $\left(\frac{x}{m}\right)_{waste}$ of ac.UWP and ac.FW/CFS indicates that the amount of ethylbenzene cracked over the activated chars produced from 1 kg of waste (225 and 239 g_{tar}/kg_{waste}, respectively) is higher than the amount of tar generated during the pyro-gasification of 1 kg of waste (210 g). On the contrary, the tar removal capacity of c.FW/CFS is insufficient to treat the tar produced by pyro-gasification, as its removal capacity was only 78 g_{tar}/kg of FW/CFS.

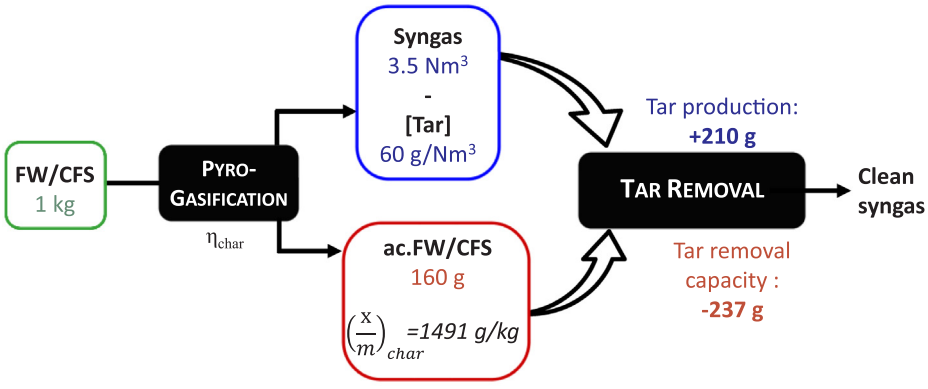

Fig. 8. Scheme of the mass balance calculations for ac.FW/CFS.

Table 5
Char yield, bulk density measured with Hg-porosimetry and tar removal capacity of the catalysts.

Catalysts	η_{char} (wt.%)	ρ_{bulk} (g/cm^3)	$\left(\frac{x}{m}\right)_{char}$ (g_{tar}/kg_{char})	$\left(\frac{x}{m}\right)_{waste}$ (g_{tar}/kg_{waste})
ac.UWP	17	0.26	1324	224
c.FW/CFS	23	0.61	340	78
ac.FW/CFS	16	0.71	1491	237

Steam activation appears as a necessary step to increase the catalytic activity of both types of chars. In addition, this process does not require the use of chemicals, and allows to obtain high char yields, defined by Eq.7. This latter is an important parameter for industrial use because a low char yield would negatively affect the economic viability of the global process.

The catalytic tests were performed with a constant catalytic bed volume in order to keep similar residence time of gas. However, the mass of catalyst used for each test varied due to the different density of the chars, as shown in Table 5. For example, the mass of ac.UWP in the catalytic bed is approximatively 2.4–2.8 times lower than that of FW/CFS-based chars. For similar weight, the two activated chars exhibit almost equivalent tar removal capacity: 1491 and 1324 g_{tar}/kg_{char} for ac.FW/CFS and ac.UWP, respectively. However, the industrial implementation of ac.FW/CFS would be easier due to its higher density. Indeed, smallest cracking reactor would be needed with this char to reach high tar removal efficiency, compared to ac.UWP. An option to reduce the volume of the tar cracking reactor with ac.UWP would consist in a particle size reduction, but this solution would drastically increase the pressure drop induced by the catalytic fixed-bed. Considering the high thermal stability and the large specific surface area developed by ac.UWP, its use as catalyst support appears as an attractive option. Moreover, a metal impregnation could significantly increase its catalytic activity and its density, thus reducing the volume of the tar cracking reactor.

4. Conclusions

This research investigated the valorisation of residual pyrolysis chars from various bio-wastes as catalysts for tar cracking. A special focus was paid to the understanding of deactivation mechanisms. Two chars were produced by the pyrolysis of bio-wastes generated in large quantities by modern societies: (1) used wood pallets (UWP), and (2) a 50/50% mixture of food waste (FW) and coagulation-flocculation sludge (CFS). The pyrolysis chars were modified without chemicals by steam activation at 850 °C. While UWP-based chars were carbonaceous materials (carbon content > 87 wt%), the FW/CFS-derived chars were hybrid carbon/mineral chars (carbon content < 44 wt%).

During ethylbenzene cracking tests at 650 °C, the activated chars were significantly more active than pyrolysis chars. Coking was responsible for the catalysts deactivation, and the textural properties strongly influenced the deactivation kinetics. High specific surface area and mesoporous volume allowed to “store” the coke in the porous surface, thus extending the catalytic efficiency of the activated chars. Micropores of the catalysts were found to be clogged faster by coke deposition than the mesopores.

For benzene conversion at 850–950 °C, hybrid carbon/mineral chars (from FW/CFS) were the most active catalysts, but the melting, diffusion and sintering of inorganic compounds at high temperature (> 850 °C) was responsible for their deactivation. Indeed, a layer composed of P and Ca with some areas rich in KCl and NaCl was deposited at the surface of FW/CFS chars after the catalytic tests at high temperature. At 950 °C, non-activated char (c.FW/CFS) was proved to be more resistant to the deactivation by inorganic species than activated char ac.FW/CFS. This extended catalytic activity was explained by two competitive effects. On the one hand, the melting, diffusion and sintering of inorganic compounds towards the surface encapsulated and covered the active mineral species. On the other hand, the activation of c.FW/CFS by the CO_2 of the syngas simultaneously developed the porosity and created new available active sites. The activated char from UWP presented lower catalytic performance and was deactivated by coke deposition. However, this material displayed high thermal stability and large specific surface area. For these reasons, ac.UWP could be an attractive material for low-cost catalyst support. This study demonstrated that the deactivation mechanisms of the chars depended on their physicochemical and thermal properties, as well as on the operating conditions. For this reason, additional experiments should be conducted to: (1) investigate the reaction and deactivation mechanisms under real syngas conditions, (2) identify the most efficient cracking temperature, (3) optimize the conditions of steam activation, and (4) find the best functionalization process for ac.UWP. Despite the significant catalytic activity of inorganic rich chars, this study proves that particular attention must be paid to the catalytic temperature at which they are used, to avoid the deactivation by melting, diffusion and sintering of inorganic species.

A proposal for process integration was presented to consider the possibility to valorise the chars as catalysts to decompose the tar generated in the same pyro-gasification process. Mass balances indicated that the tar removal capacity of both activated chars was sufficient to remove the tar generated by the pyro-gasification process. The industrial implementation of ac.FW/CFS would be easier than that of ac.UWP due to its higher density, allowing to design smaller cracking reactor. The promising results obtained in this study demonstrated that pyrolysis chars from bio-wastes could be valorised *in-situ* as efficient, low-cost and eco-friendly catalysts for tar cracking and syngas cleaning.

Acknowledgement

This research was supported by the ANR Carnot M.I.N.E.S (CHARPURGAS grant 30530). The authors acknowledge the technical staff of IMT Atlantique Mines Nantes (Yvan Gouriou, Eric Chevrel, François-Xavier Blanchet, Jérôme Martin), Mines Albi (Nathalie Lyczko, Laurène Haurie, Sylvie Del-Confetto, Mickaël Ribeiro, Pierre Bertorelle and Denis Marty) for assistance with experiments and analyses.

Appendix A. Supplementary material

Supplementary data to this article can be found online at https://doi.org/10.1016/j.apenergy.2019.01.021.

References

[1] Arena U. Process and technological aspects of municipal solid waste gasification. A review. Waste Manag 2012;32:625–39. https://doi.org/10.1016/j.wasman.2011.09.025.
[2] Bridgwater AV. Review of fast pyrolysis of biomass and product upgrading. Biomass Bioenergy 2012;38:68–94. https://doi.org/10.1016/j.biombioe.2011.01.048.
[3] Berhanu S, Hervy M, Weiss-Hortala E, Proudhon H, Berger M-H, Chesnaud A, et al. Advanced characterization unravels the structure and reactivity of wood-based chars. J Anal Appl Pyrol 2018;130:79–89. https://doi.org/10.1016/j.jaap.2018.01.024.
[4] Hervy M, Berhanu S, Weiss-Hortala E, Chesnaud A, Gérente C, Villot A, et al. Multi-scale characterisation of chars mineral species for tar cracking. Fuel 2017;189:88–97. https://doi.org/10.1016/j.fuel.2016.10.089.
[5] Woolcock PJ, Brown RC. A review of cleaning technologies for biomass-derived syngas. Biomass Bioenergy 2013;52:54–84. https://doi.org/10.1016/j.biombioe.2013.02.036.
[6] Milne TA, Evans R, Abatzoglou N. Biomass gasifier tars: their nature, formation and conversion. National Renewable Energy Laboratory; 1998.
[7] Nakamura S, Kitano S, Yoshikawa K. Biomass gasification process with the tar removal technologies utilizing bio-oil scrubber and char bed. Appl Energy 2016;170:186–92. https://doi.org/10.1016/j.apenergy.2016.02.113.
[8] Font Palma C. Modelling of tar formation and evolution for biomass gasification: a review. Appl Energy 2013;111:129–41. https://doi.org/10.1016/j.apenergy.2013.04.082.
[9] Burhenne L, Aicher T. Benzene removal over a fixed bed of wood char: the effect of

pyrolysis temperature and activation with CO2 on the char reactivity. Fuel Process Technol 2014;127:140–8. https://doi.org/10.1016/j.fuproc.2014.05.034.
[10] Shen Y, Zhao P, Shao Q, Takahashi F, Yoshikawa K. In situ catalytic conversion of tar using rice husk char/ash supported nickel–iron catalysts for biomass pyrolytic gasification combined with the mixing-simulation in fluidized-bed gasifier. Appl Energy 2015;160:808–19. https://doi.org/10.1016/j.apenergy.2014.10.074.
[11] Le Coq L, Duga A. Syngas treatment unit for small scale gasification-application to IC engine gas quality requirement. J Appl Fluid Mech 2012;5:95–103.
[12] Phuphuakrat T, Namioka T, Yoshikawa K. Tar removal from biomass pyrolysis gas in two-step function of decomposition and adsorption. Appl Energy 2010;87:2203–11. https://doi.org/10.1016/j.apenergy.2009.12.002.
[13] Bergman PC, van Paasen SV, Boerrigter H. The novel "OLGA" technology for complete tar removal from biomass producer gas. In: Pyrolysis Gasif. Biomass Waste Expert Meet. Strasbg. Fr.; 2002. < https://www.ecn.nl/fileadmin/ecn/units/bio/Overig/pdf/Olga4.pdf > [accessed July 6, 2016].
[14] Zwart RWR, Van der Drift A, Bos A, Visser HJM, Cieplik MK, Könemann HWJ. Oil-based gas washing—flexible tar removal for high-efficient production of clean heat and power as well as sustainable fuels and chemicals. Environ Prog Sustain Energy 2009;28:324–35. https://doi.org/10.1002/ep.10383.
[15] Villot A, Gonthier Y, Gonze E, Bernis A, Ravel S, Grateau M, et al. Separation of particles from syngas at high-temperatures with an electrostatic precipitator. Sep Purif Technol 2012;92:181–90. https://doi.org/10.1016/j.seppur.2011.04.028.
[16] Nair SA, Pemen AJM, Yan K, van Gompel FM, van Leuken HEM, van Heesch EJM, et al. Tar removal from biomass-derived fuel gas by pulsed corona discharges. Fuel Process Technol 2003;84:161–73. https://doi.org/10.1016/S0378-3820(03)00053-5.
[17] Houben MP, de Lange HC, van Steenhoven AA. Tar reduction through partial combustion of fuel gas. Fuel 2005;84:817–24. https://doi.org/10.1016/j.fuel.2004.12.013.
[18] Tsuboi Y, Ito S, Takafuji M, Ohara H, Fujimori T. Development of a regenerative reformer for tar-free syngas production in a steam gasification process. Appl Energy 2017;185:1217–24. https://doi.org/10.1016/j.apenergy.2015.12.110.
[19] Fagbemi L, Khezami L, Capart R. Pyrolysis products from different biomasses: application to the thermal cracking of tar. Appl Energy 2001;69:293–306. https://doi.org/10.1016/S0306-2619(01)00013-7.
[20] Shen Y, Yoshikawa K. Recent progresses in catalytic tar elimination during biomass gasification or pyrolysis—a review. Renew Sustain Energy Rev 2013;21:371–92. https://doi.org/10.1016/j.rser.2012.12.062.
[21] Wang D, Yuan W, Ji W. Char and char-supported nickel catalysts for secondary syngas cleanup and conditioning. Appl Energy 2011;88:1656–63. https://doi.org/10.1016/j.apenergy.2010.11.041.
[22] Constantinou DA, Fierro JLG, Efstathiou AM. A comparative study of the steam reforming of phenol towards H_2 production over natural calcite, dolomite and olivine materials. Appl Catal B Environ 2010;95:255–69. https://doi.org/10.1016/j.apcatb.2010.01.003.
[23] Chen J, Tamura M, Nakagawa Y, Okumura K, Tomishige K. Promoting effect of trace Pd on hydrotalcite-derived Ni/Mg/Al catalyst in oxidative steam reforming of biomass tar. Appl Catal B Environ 2015;179:412–21. https://doi.org/10.1016/j.apcatb.2015.05.042.
[24] Brandt P, Larsen E, Henriksen U. High tar reduction in a two-stage gasifier. Energy Fuels 2000;14:816–9. https://doi.org/10.1021/ef990182m.
[25] Guan G, Chen G, Kasai Y, Lim EWC, Hao X, Kaewpanha M, et al. Catalytic steam reforming of biomass tar over iron- or nickel-based catalyst supported on calcined scallop shell. Appl Catal B Environ 2012;115–116:159–68. https://doi.org/10.1016/j.apcatb.2011.12.009.
[26] Hervy M, Pham Minh D, Gérente C, Weiss-Hortala E, Nzihou A, Villot A, et al. removal from syngas using wastes pyrolysis chars. Chem Eng J 2018;334:2179–89. https://doi.org/10.1016/j.cej.2017.11.162.
[27] Abu El-Rub Z, Bramer EA, Brem G. Experimental comparison of biomass chars with other catalysts for tar reduction. Fuel 2008;87:2243–52. https://doi.org/10.1016/j.fuel.2008.01.004.
[28] Al-Rahbi AS, Williams PT. Hydrogen-rich syngas production and tar removal from biomass gasification using sacrificial tyre pyrolysis char. Appl Energy 2017;190:501–9. https://doi.org/10.1016/j.apenergy.2016.12.099.
[29] Ravenni G, Sárossy Z, Ahrenfeldt J, Henriksen UB. Activity of chars and activated carbons for removal and decomposition of tar model compounds – a review. Renew Sustain Energy Rev 2018;94:1044–56. https://doi.org/10.1016/j.rser.2018.07.001.
[30] Zhang S, Asadullah M, Dong L, Tay H-L, Li C-Z. An advanced biomass gasification technology with integrated catalytic hot gas cleaning. Part II: Tar reforming using char as a catalyst or as a catalyst support. Fuel 2013;112:646–53. https://doi.org/10.1016/j.fuel.2013.03.015.
[31] Guo F, Li X, Liu Y, Peng K, Guo C, Rao Z. Catalytic cracking of biomass pyrolysis tar over char-supported catalysts. Energy Convers Manag 2018;167:81–90. https://doi.org/10.1016/j.enconman.2018.04.094.
[32] Hu M, Laghari M, Cui B, Xiao B, Zhang B, Guo D. Catalytic cracking of biomass tar over char supported nickel catalyst. Energy 2018;145:228–37. https://doi.org/10.1016/j.energy.2017.12.096.
[33] Klinghoffer NB, Castaldi MJ, Nzihou A. Catalyst properties and catalytic performance of char from biomass gasification. Ind Eng Chem Res 2012;51:13113–22. https://doi.org/10.1021/ie3014082.
[34] Xiong X, Yu IKM, Cao L, Tsang DCW, Zhang S, Ok YS. A review of biochar-based catalysts for chemical synthesis, biofuel production, and pollution control. Bioresour Technol 2017;246:254–70. https://doi.org/10.1016/j.biortech.2017.06.163.
[35] Bartholomew CH. Mechanisms of catalyst deactivation. Appl Catal Gen 2001;212:17–60. https://doi.org/10.1016/S0926-860X(00)00843-7.
[36] Hosokai S, Norinaga K, Kimura T, Nakano M, Li C-Z, Hayashi J. Reforming of volatiles from the biomass pyrolysis over charcoal in a sequence of coke deposition and steam gasification of coke. Energy Fuels 2011;25:5387–93. https://doi.org/10.1021/ef2003766.
[37] Lu P, Huang Q, Chi Y, Yan J. Preparation of high catalytic activity biochar from biomass waste for tar conversion. J Anal Appl Pyrol 2017;127:47–56. https://doi.org/10.1016/j.jaap.2017.09.003.
[38] Dufour A, Celzard A, Fierro V, Broust F, Courson C, Zoulalian A, et al. Catalytic conversion of methane over a biomass char for hydrogen production: deactivation and regeneration by steam gasification. Appl Catal Gen 2015;490:170–80. https://doi.org/10.1016/j.apcata.2014.10.038.
[39] Rostrup-Nielsen JR. Industrial relevance of coking. Catal Today 1997;37:225–32. https://doi.org/10.1016/S0920-5861(97)00016-3.
[40] Xiao X, Meng X, Le DD, Takarada T. Two-stage steam gasification of waste biomass in fluidized bed at low temperature: parametric investigations and performance optimization. Bioresour Technol 2011;102:1975–81. https://doi.org/10.1016/j.biortech.2010.09.016.
[41] Zhang Y, Kajitani S, Ashizawa M, Oki Y. Tar destruction and coke formation during rapid pyrolysis and gasification of biomass in a drop-tube furnace. Fuel 2010;89:302–9. https://doi.org/10.1016/j.fuel.2009.08.045.
[42] Nzihou A, Stanmore B, Sharrock P. A review of catalysts for the gasification of biomass char, with some reference to coal. Energy 2013;58:305–17. https://doi.org/10.1016/j.energy.2013.05.057.
[43] Park SY, Oh G, Kim K, Seo MW, Ra HW, Mun TY, et al. Deactivation characteristics of Ni and Ru catalysts in tar steam reforming. Renew Energy 2017;105:76–83. https://doi.org/10.1016/j.renene.2016.12.045.
[44] Dufour A, Masson E, Girods P, Rogaume Y, Zoulalian A. Evolution of aromatic tar composition in relation to methane and ethylene from biomass pyrolysis-gasification. Energy Fuels 2011;25:4182–9. https://doi.org/10.1021/ef200846g.
[45] Morgalla M, Lin L, Strand M. Decomposition of benzene using char aerosol particles dispersed in a high-temperature filter. Energy 2017;118:1345–52. https://doi.org/10.1016/j.energy.2016.11.016.
[46] Gilbert P, Ryu C, Sharifi V, Swithenbank J. Tar reduction in pyrolysis vapours from biomass over a hot char bed. Bioresour Technol 2009;100:6045–51. https://doi.org/10.1016/j.biortech.2009.06.041.
[47] Wang N, Chen D, Arena U, He P. Hot char-catalytic reforming of volatiles from MSW pyrolysis. Appl Energy 2017;191:111–24. https://doi.org/10.1016/j.apenergy.2017.01.051.
[48] Molina-Sabio M, Gonzalez MT, Rodriguez-Reinoso F, Sepúlveda-Escribano A. Effect of steam and carbon dioxide activation in the micropore size distribution of activated carbon. Carbon 1996;34:505–9. https://doi.org/10.1016/0008-6223(96)00006-1.
[49] Mohamad Nor N, Lau LC, Lee KT, Mohamed AR. Synthesis of activated carbon from lignocellulosic biomass and its applications in air pollution control—a review. J Environ Chem Eng 2013;1:658–66. https://doi.org/10.1016/j.jece.2013.09.017.
[50] Dupont C, Jacob S, Marrakchy KO, Hognon C, Grateau M, Labalette F, et al. How inorganic elements of biomass influence char steam gasification kinetics. Energy 2016;109:430–5. https://doi.org/10.1016/j.energy.2016.04.094.
[51] Wang F-J, Zhang S, Chen Z-D, Liu C, Wang Y-G. Tar reforming using char as catalyst during pyrolysis and gasification of Shengli brown coal. J Anal Appl Pyrol 2014;105:269–75. https://doi.org/10.1016/j.jaap.2013.11.013.
[52] Zhang Y, Ashizawa M, Kajitani S, Miura K. Proposal of a semi-empirical kinetic model to reconcile with gasification reactivity profiles of biomass chars. Fuel 2008;87:475–81. https://doi.org/10.1016/j.fuel.2007.04.026.
[53] Yildiz G, Ronsse F, Venderbosch R, van Duren R, Kersten SRA, Prins W. Effect of biomass ash in catalytic fast pyrolysis of pine wood. Appl Catal B Environ 2015;168–169:203–11. https://doi.org/10.1016/j.apcatb.2014.12.044.
[54] Dupont C, Nocquet T, Da Costa JA, Verne-Tournon C. Kinetic modelling of steam gasification of various woody biomass chars: influence of inorganic elements. Bioresour Technol 2011;102:9743–8. https://doi.org/10.1016/j.biortech.2011.07.016.
[55] Asadullah M, Zhang S, Min Z, Yimsiri P, Li C-Z. Effects of biomass char structure on its gasification reactivity. Bioresour Technol 2010;101:7935–43. https://doi.org/10.1016/j.biortech.2010.05.048.
[56] Guo J, Luo Y, Lua AC, Chi R, Chen Y, Bao X, et al. Adsorption of hydrogen sulphide (H_2S) by activated carbons derived from oil-palm shell. Carbon 2007;45:330–6. https://doi.org/10.1016/j.carbon.2006.09.016.
[57] Maschio G, Lucchesi A, Stoppato G. Production of syngas from biomass. Bioresour Technol 1994;48:119–26.
[58] Wei L, Xu S, Zhang L, Liu C, Zhu H, Liu S. Steam gasification of biomass for hydrogen-rich gas in a free-fall reactor. Int J Hydrog Energy 2007;32:24–31. https://doi.org/10.1016/j.ijhydene.2006.06.002.
[59] Hervy M, Villot A, Gérente C, Pham Minh D, Weiss-Hortala E, Nzihou A, et al. Catalytic cracking of ethylbenzene as tar surrogate using pyrolysis chars from wastes. Biomass Bioenergy 2018;117:86–95. https://doi.org/10.1016/j.biombioe.2018.07.020.
[60] Morgalla M, Lin L, Strand M. Benzene conversion in a packed bed loaded with biomass char particles. Energy Fuels 2017. https://doi.org/10.1021/acs.energyfuels.7b03236.
[61] Drago RS, Jurczyk K. Oxidative dehydrogenation of ethylbenzene to styrene over carbonaceous catalysts. Appl Catal Gen 1994;112:117–24. https://doi.org/10.1016/0926-860X(94)80213-0.
[62] Moliner R, Suelves I, Lázaro MJ, Moreno O. Thermocatalytic decomposition of methane over activated carbons: influence of textural properties and surface chemistry. Int J Hydrog Energy 2005;30:293–300. https://doi.org/10.1016/j.ijhydene.2004.03.035.

[63] Sueyasu T, Oike T, Mori A, Kudo S, Norinaga K, Hayashi J. Simultaneous steam reforming of tar and steam gasification of char from the pyrolysis of potassium-loaded woody biomass. Energy Fuels 2012;26:199–208. https://doi.org/10.1021/ef201166a.
[64] Hayashi J-I, Iwatsuki M, Morishita K, Tsutsumi A, Li C-Z, Chiba T. Roles of inherent metallic species in secondary reactions of tar and char during rapid pyrolysis of brown coals in a drop-tube reactor. Fuel 2002;81:1977–87. https://doi.org/10.1016/S0016-2361(02)00128-X.
[65] Hognon C, Dupont C, Grateau M, Delrue F. Comparison of steam gasification reactivity of algal and lignocellulosic biomass: influence of inorganic elements. Bioresour Technol 2014;164:347–53. https://doi.org/10.1016/j.biortech.2014.04.111.
[66] Sevonius C, Yrjas P, Hupa M. Defluidization of a quartz bed – laboratory experiments with potassium salts. Fuel 2014;127:161–8. https://doi.org/10.1016/j.fuel.2013.10.047.
[67] Balland M. Gazéification de biomasse en lit fluidisé: étude phénoménologique de l'agglomération liée à la fusion des cendres. Phd thesis. Université d'Orléans; 2016. < https://tel.archives-ouvertes.fr/tel-01407243/document > [accessed November 26, 2018].
[68] Khan AA, de Jong W, Jansens PJ, Spliethoff H. Biomass combustion in fluidized bed boilers: potential problems and remedies. Fuel Process Technol 2009;90:21–50. https://doi.org/10.1016/j.fuproc.2008.07.012.
[69] Niu Y, Zhu Y, Tan H, Hui S, Jing Z, Xu W. Investigations on biomass slagging in utility boiler: criterion numbers and slagging growth mechanisms. Fuel Process Technol 2014;128:499–508.
[70] Van der Drift A, Olsen A. Conversion of boimass prediction and solution methods for ash agglomeration and related problems. ECN 1999.
[71] Devi L, Ptasinski KJ, Janssen FJJG. A review of the primary measures for tar elimination in biomass gasification processes. Biomass Bioenergy 2003;24:125–40. https://doi.org/10.1016/S0961-9534(02)00102-2.
[72] Dufour A, Celzard A, Fierro V, Martin E, Broust F, Zoulalian A. Catalytic decomposition of methane over a wood char concurrently activated by a pyrolysis gas. Appl Catal Gen 2008;346:164–73. https://doi.org/10.1016/j.apcata.2008.05.023.
[73] Jenbacher GE. Fuel gas quality, special gases; 2009.